FlatChem 38 (2023) 100470

Contents lists available at ScienceDirect

FlatChem

journal homepage: www.sciencedirect.com/journal/flatchem

Bulk substitution of F-terminations from $Ti_3C_2T_x$ MXene by cation pillaring and gas hydrolysation

Frode Håskjold Fagerli [a], Per Erik Vullum [b,c], Tor Grande [a], Zhaohui Wang [a,b], Sverre M. Selbach [a], Kjell Wiik [a], Nils Peter Wagner [a,b,*]

[a] Department of Materials Science and Engineering, Norwegian University of Science and Technology, NO-7034 Trondheim, Norway
[b] SINTEF Industry, NO-7034 Trondheim, Norway
[c] Department of Physics, Norwegian University of Science and Technology, NO-7034 Trondheim, Norway

ARTICLE INFO

Keywords:
MXene
Surface terminations
Hydrolysis
2D material
LiB

ABSTRACT

Applications of 2D MXenes are limited by the difficulty of controlling bulk termination groups after the initial HF etching step without forming surface oxides. Here, we report on gas hydrolysation using a continuous flow of Ar (g) with a controlled partial pressure of H_2O (g) as a new method to change the terminations of multilayered $Ti_3C_2T_x$ MXene particles (T = O, OH and F), and demonstrate pre-intercalation of cations as a necessity for successful hydrolysation as it enables water molecules to enter the $Ti_3C_2T_x$ MXene structure. Hydrolysation of pristine HF-etched $Ti_3C_2T_x$ shows no compositional change before oxidation into a TiO_2/C composite starts at T > 300 °C. However, by pre-intercalating various cations into the MXene, a pillaring of the structure is achieved, which for certain cations (K^+ and Na^+) remains even after hydrolysation at 300 °C. By hydrolysing K-intercalated $Ti_3C_2T_x$ at 300 °C, a significant bulk F reduction of 78 % was achieved, accompanied by a comparable increase in O content and insignificant surface oxidation of the particles. For other cations (Mg^{2+}, Li^+ and TBA^+) the expanded interlayer spacing collapsed upon hydrolysation, resulting in no significant compositional changes. Moreover, hydrolysation is shown to give higher selectivity towards F removal compared to air annealing, which instead resulted in the oxidation of C to CO_2 and the formation of $TiOF_2$. In Li-ion battery half cells, the intercalation of K-ions reduces both the capacity and energy efficiency compared to pristine $Ti_3C_2T_x$. Nevertheless, hydrolysation increases the capacity and intercalation voltage, and is thus a feasible method to control the electrochemical performance of $Ti_3C_2T_x$ MXene. In summary, gas hydrolysation is demonstrated as a selective and efficient method to substitute F terminations with O-related terminations in multilayered MXene particles and pave the way for utilisation on other MXene compositions.

1. Introduction

MXenes are 2D materials with properties suitable for a wide range of applications, e.g. from electrochemical interference shielding and sensors to water desalination and biomedicine.[1–4] Consisting of transition metals 'M', and C and/or N as the 'X' element in a layered structure of $M_{y+1}X_y$ (y = 1, 2, 3, 4), these materials have demonstrated high electrical conductivity and intercalation capability for several cations, making them especially interesting as electrode materials in batteries and supercapacitors.[5–7] However, to optimise the intercalation properties of MXenes, control of their chemical composition is necessary. While the M and X elements can be controlled by choosing the correct MAX phase precursor, a mixture of surface terminations (T) are formed on the 2D sheets during synthesis, which is denoted by "T_x" (i.e., $Ti_3C_2T_x$).[8] So far, mainly -O, –OH and -F terminations stemming from etching in aqueous HF or HF forming solutions have been studied.[9,10] The combination of these termination groups is expected to greatly influence the intercalating properties, and DFT calculations predict higher capacities, lower migration barriers and higher open circuit voltages for O-terminated surfaces compared to F-terminated surfaces.[11–14] Control of termination groups is thus a key challenge for further development of MXenes in general, and especially for rechargeable batteries.[8,15].

Although the importance of termination control has been known for a decade, only limited progress has been made. In recent years, alternative etching methods based on anhydrous halogen solutions, molten

* Corresponding author.
E-mail address: nils.peter.wagner@sintef.no (N.P. Wagner).

https://doi.org/10.1016/j.flatc.2023.100470
Received 8 September 2022; Received in revised form 30 November 2022; Accepted 4 January 2023
Available online 6 January 2023

salt reactions and hydrothermal etching in NaOH solutions have been developed, and have resulted in homogeneously terminated $Ti_3C_2T_x$ MXene (i.e. -S, -Se, -Br, -Cl, -O).[16–19] However, as HF etching remains the most scalable synthesis method, post-etching modification of the termination groups would accelerate the development of MXenes for batteries. Considering the most studied $Ti_3C_2T_x$ phase, one of the major challenges is related to its poor oxidative stability, as it oxidises into TiO_2 at elevated temperatures in both inert, reducing and oxidising atmospheres, as well as in aqueous dispersions.[20–23] However, changing the composition from $Ti_3C_2F_2$ to $Ti_3C_2O_2$ must be charge compensated by oxidation of the MXene. Therefore, controlling the selectivity of the chemical reactions upon post-etching treatments is essential to control the termination change while preventing oxidation into TiO_2 phases.

Previously reported methods to control the surface terminations include annealing in vacuum, CO_2, O_2, H_2 and inert atmospheres,[21,24–26] dispersion in alkalic and acidic solutions,[27–29] as well as hydrothermal treatment.[25] Most of these methods do not reduce the F-content without the surface oxidizing into TiO_2. The results from Halim et al. indicate stable MXene thin films upon annealing at 550 ℃ in ultrahigh vacuum, which also resulted in a removal of most of the initial F content.[24] Howbeit, to date this method has only been demonstrated for thin films of unspecified thickness and not for multilayered MXene particles. Considering the chemistry of the F-removal, it seems unlikely that F-terminations will leave the MXene as F-ions or F_2 gas, as it would either require an electrical instability in the remaining MXene or a strong oxidation of the F-terminations. We recently reported on gas hydrolysation as a new method to remove F-terminations from V_2CT_x MXene by the formation of HF gas,[30] and now we apply a similar approach to control the terminations in $Ti_3C_2T_x$ - one of the most studied MXene phases.

In this article, we report the structural and compositional changes in multilayered $Ti_3C_2T_x$ particles from gas hydrolysation and demonstrate the essential role of cation intercalation prior to the hydrolysis. First, density functional theory (DFT) calculations on possible hydrolysation reactions are presented, guiding the experimental hydrolysation of pristine HF-etched $Ti_3C_2T_x$ MXene up to 500 ℃. These results are then compared with annealing in various atmospheres to identify differences in thermal stability and selectivity towards F-removal. Thereafter, intercalation of Li-, Na-, K-, Mg- and tetrabutylammonion-ions (TBA) as pillars for the MXene layers are demonstrated together with the changes upon subsequent gas hydrolysation. Finally, electrochemical cycling results from intercalated and hydrolysed MXenes are presented. To verify the bulk compositional changes within the particles, comprehensive characterization by energy dispersive X-ray spectroscopy (EDS) is performed with an electron acceleration voltage of 10 kV to ensure a data acquisition depth of $>$ 300 nm.[31].

2. Methods

2.1. Synthesis of $Ti_3C_2T_x$

Prior to the etching, commercial Ti_3AlC_2 MAX phase powder (Laizhou Kai Kai Ceramic Materials Co., ltd.) was planetary milled at 300 rpm for 150 min in isopropanol with the use of WC milling jar and balls, to obtain a small and controlled particle size and particle size distribution (Figure S1). Then, 2.5 g of the milled powder was slowly added over 15 min to a polypropylene beaker with 50 mL of a 10 wt% HF solution, before the beaker was partly covered with parafilm and left at room temperature for 24 h under constant stirring. After the etching, the remaining powder dispersion was washed several times by centrifugation and decantation in DI-water dispersions until a pH $>$ 5 was reached. Thereafter, the remaining dispersion was vacuum filtered through 0.22 μm pore sized PVDF filter papers, before the powder was vacuum dried at 60 ℃ for 4 h and the pristine $Ti_3C_2T_x$ powder was obtained.

2.2. Cation intercalation

The different cations were intercalated by dispersing 0.4 g of the $Ti_3C_2T_x$ powder in 50 mL salt solutions under constant agitation before washing the powder several times with DI water by centrifugation. Lastly, the powders were vacuum filtered and dried under vacuum at 40 ℃ for up to 1 h. TBA-Ti_3C_2 was prepared by dispersing $Ti_3C_2T_x$ in a 1.2 M TBAOH solution over 12 h, while K-Ti_3C_2, Na-Ti_3C_2, and Li-Ti_3C_2 were made using 2 M hydroxide solutions for 2 h. Mg-Ti_3C_2, was made by substituting the Na-ions from Na-Ti_3C_2. This was done by adding the Na-Ti_3C_2 powder to a 1 M $MgCl_2$ solution for 3 h, before the powder was washed in DI water and left for another 20 h in a fresh $MgCl_2$ solution.

2.3. Hydrolysation and annealing

Gas hydrolysation was performed as previously described [30] by distributing 0.1 g powder over 1–2 cm^2 in an alumina crucible followed by 2 hrs with 200 mL/min Ar gas (99.999 %) flushing in a quartz tube furnace. Heating rates were kept at 300 ℃/h followed by 15 hrs dwell time with the same gas flow. The Hyd300C notation indicates the hydrolysation temperature that was used, which in this case was 300 ℃. The Ar gas was bubbled through a DI water bath, which after the flushing step was heated to and kept at a temperature of 80 ℃. This results in a saturated vapor pressure of 0.474 bar.[32] To prevent air leakage into the furnace and to capture HF formed during the hydrolysation, the exhaust gas was bubbled through a solution of 1 M Ca $(NO_3)_2$. For Air-Ti_3C_2, Ar-Ti_3C_2, Ar/H_2-Ti_3C_2 and Vac-Ti_3C_2 the annealing gases were dry synthetic air, pure Ar gas (99.999 %), a 5 % H_2 mixture in pure Ar gas and a pressure of $<$ 1 mbar, respectively. Annealing was done with the same heating parameters as for the hydrolysation.

2.4. Characterization techniques

Crystal structure and phase purity were characterized by X-ray powder diffraction (XRD, Bruker D8 Focus Diffractometer) using a 0.2 mm slit size and a Cu Kα radiation source ($\lambda = 0.15406$ nm). The XRD data were collected with a step size of 0.0143° and a 0.68 s step time in a 2θ-range from 4 to 75°, and the resulting diffractograms were adjusted for sample displacement by structureless fitting in the TOPAS software using a $P6_3/mmc$ space group (Figure S3). The particle size distribution (PSD) of the MAX phase was measured by laser diffraction (Horiba Partica LA-960) in isopropanol dispersions. The microstructure and surface morphology of the particles were investigated by a field-emission scanning electron microscope (FESEM, Carl Zeiss Ag – ULTRA 55) using an acceleration voltage of 5 kV. Energy dispersive X-ray spectroscopy (EDS) was used to assess chemical composition using an XFlash 4010 X-ray detector and an acceleration voltage of 10 kV, resulting in an electron penetration depth $>$ 300 nm for $Ti_3C_2T_x$ with a density of around 4.2 g/cm^3.[31] To obtain quantitative results, the point scans were analysed using the Bruker Esprit 1.9 software, and the average values from minimum six point scans with a tilt $<$ 32° relative to the detector were used for each material (Figure S2 and Table S1). The vibrational properties were investigated by a WITec Alpha 300r Confocal Raman Microscope, using a 100x objective, a 532 nm Ar laser and a laser power below 0.8 mW to prevent oxidation of the material.[33] Additionally, Fourier-transform Infrared spectroscopy (FTIR, Bruker VERTEX 80v) Drifts measurements were performed at 2 mBar using KBr powder both as reference and for the sample mixture in a MXene:KBr mass ratio of 1:39. Transmission electron microscopy (TEM) was performed with a double Cs aberration corrected cold FEG Jeol ARM200FC, operated at 200 kV. EDS maps were acquired in scanning TEM (STEM) mode with a 100 mm^2 Centurio detector, covering a solid angle of 0.98 sr. The TEM samples were prepared perpendicular to the (0 0 2) plane by focused ion beam (FIB) lamella preparation, using a Helios G4 UX. All coarse thinning of the lamellae were done with 30 kV

acceleration voltage for the Ga^+ ions. Final thinning was done at 5 kV and then at 2 kV on either side of the lamellae to minimize surface damage.

2.5. Electrochemical measurements

To assess the electrochemical performance of the hydrolysed $Ti_3C_2T_x$, Li-ion battery half cells were prepared with MXene particles as the working electrode. These electrodes were processed by mixing *N*-ethyl-2-pyrrolidone (NEP)-slurries with 10 wt% carbon black as conductive additive, 10 wt% PVDF binder and 80 wt% of the active material (various compositions of $Ti_3C_2T_x$). First the carbon black and active material were mixed in a shaker mill for 10 min at 25 Hz. Then, a premade PVDF-NEP solution was added before the slurry was further diluted with additional NEP to obtain a solid to liquid ratio of 1:6. Next, the slurry was mixed by continued shaking for 30 min at 15 Hz with a shaker ball and drop cast onto pre-cut circular Cu current collectors with a 16 mm diameter. The electrodes were dried on a 60 ℃ hot plate in a fume hood overnight before being dried under vacuum at 60 ℃ for a minimum of 3 h. This resulted in active material loadings of 1.8–2.8 mg/cm^2. The electrodes were assembled into 2016-type coin cells in an argon-filled glovebox ($O_2 \leq 0.1$ ppm, $H_2O \leq 0.1$ ppm) using Li-foil as the counter electrode, glass microfiber (Whatman) separator soaked in 110 μL 1 M $LiPF_6$ in ethylene carbonate and ethyl methyl carbonate (EC:EMC 1:1 v:v) electrolyte. The assembled cells were galvanostatically cycled in a voltage range of 0.001 to 3.0 V at various specific currents (10 mA/g-400 mA/g) using BioLogic BCS-805 and Landt CT2001A cyclers at a controlled temperature of 25 ℃.

2.6. Theoretical calculations

Density functional theory calculations were carried out with VASP using the PBEsol functional.[34–36] The Ti_pv and standard C, O, H, F pseudopotensials supplied with VASP were used and the plane-wave energy cut-off was set to 650 eV. Geometries were relaxed until the forces on the ions were below 10^{-4} eV/Å to obtain ground state energies (E0(T = 0 K)), and for solid structures gamma-centred k-point meshes with ~0.2 $Å^{-1}$ spacings were used. Vibrational properties for gases were calculated by standard statistical mechanics,[37] and for solids phases with Phonopy.[38] Corresponding zero-point energies (ZPE) were calculated for the solids and taken from the NIST-CCCBDB database for gaseous species.[39] More details about the computational methods can be found in our previous work.[30].

3. Results and discussion

3.1. DFT calculations of hydrolysation reactions

To investigate if the substitution of F terminations by hydrolysation would be feasible from a thermodynamic point of view, the change in Gibbs free energy for two different hydrolysation reactions were calculated. The results are given in Fig. 1 and show how the formation of $Ti_3C_2O_2$ is favoured compared to the formation of $Ti_3C_2(OH)_2$. While the formation of $Ti_3C_2(OH)_2$ has a positive ΔG° for all temperatures, the O-termination reaction shows a negative ΔG° at T > 400 K. However, under non-standard conditions, ΔG will be affected by the ratio between the vapour pressure of H_2O and HF, where an excess H_2O will help to shift both reactions towards the product side. In Fig. 1b, the equilibrium partial pressure of HF gas is presented as a function of temperature, assuming a constant high water vapour pressure of 0.473 bar. It shows that a significant amount of HF gas (> 40 Pa) could be formed for both reactions at a temperature of 300 ℃ (573 K), where the $Ti_3C_2O_2$ forming reaction shows the highest vapour pressure of 4000 Pa (0.04 bar). These thermodynamic results resemble what was found for the hydrolysis of V_2CT_x MXene, where a significant reduction of F content also was achieved experimentally.[30] Similarly for the $Ti_3C_2T_x$ MXene phase, substitution of F- with O containing terminations should be possible from a thermodynamic point of view. The DFT results also demonstrate how the hydrolysation would favour formation of O-terminations over OH-terminations.

3.2. Hydrolysation of pristine $Ti_3C_2T_x$

To assess if hydrolysis could alter the termination groups experimentally, HF-etched $Ti_3C_2T_x$ MXene (Figure S4) with mixed terminations was hydrolysed at various temperatures, using long hydrolysation times of 15 h to allow for complete reactions. In Fig. 2, the structural and vibrational changes of the pristine $Ti_3C_2T_x$ MXene after hydrolysation at temperatures up to 500 ℃ are presented. The X-ray diffractograms in Fig. 2a demonstrate how the $Ti_3C_2T_x$ phase remains stable up to 300 ℃, while the (101) reflection of anatase at 25.3° appears at higher temperatures. After hydrolysation at 500 ℃, the MXene phase is completely decomposed into three different TiO_2 phases (anatase, rutile and brookite) in roughly a 1:1:1 ratio (Figure S5a). The oxidation of $Ti_3C_2T_x$ is also confirmed by the vibrational spectra (Fig. 2b and c), demonstrating an additional shoulder of Ti-O bonds above 300 ℃ in the FTIR spectra, and TiO_2 anatase peaks above 400 ℃ in the Raman spectra. These spectroscopic results also present the formation of disordered graphitic carbon, as the D and G Raman bands at 1345 cm^{-1} and 1595 cm^{-1} show a cumulative intensity ratio of $I_D/I_G > 1$ indicative of

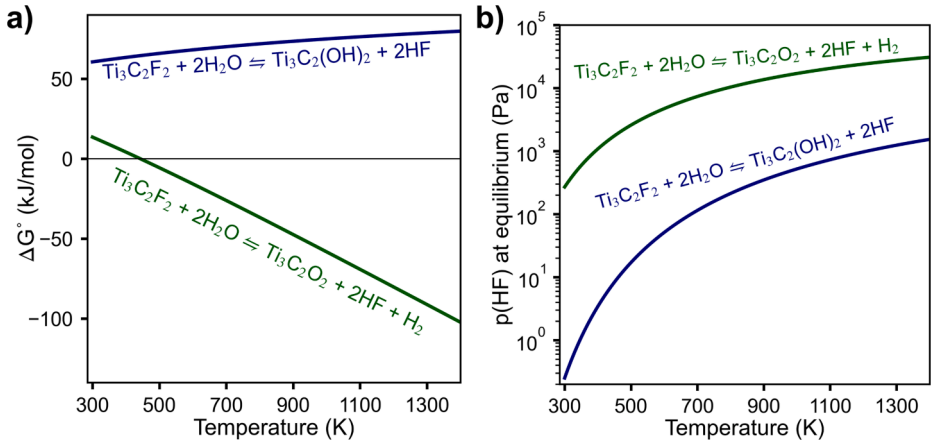

Fig. 1. DFT results for two different F-removing hydrolysation reactions for $Ti_3C_2T_x$, where (a) shows ΔG° as a function of temperature and (b) shows the equilibrium partial pressure of HF gas as a function of temperature, using a high partial pressure of H_2O (0.474 bar).

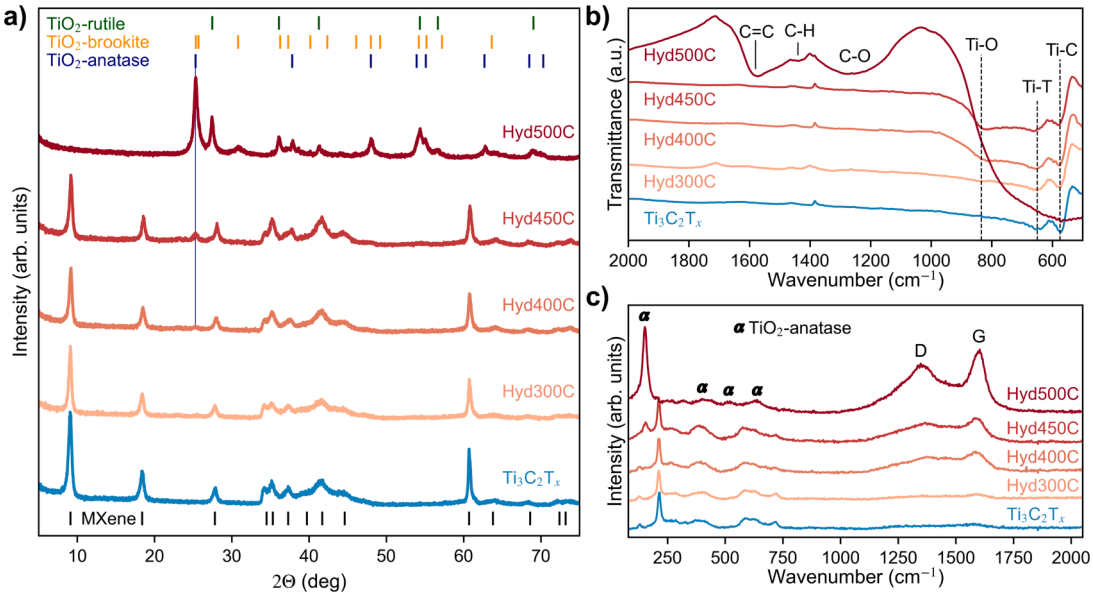

Fig. 2. XRD diffractograms (a), Raman spectra (b) and FTIR spectra (c) of $Ti_3C_2T_x$ before and after hydrolysation at various temperatures. The peaks at around 1380 cm^{-1} in the FTIR spectra come from impurities in the measurement chamber, and the (*hkl*) MXene reflections in (a) are labelled in Figure S4.

amorphous carbon,[40,41] and the various carbon-related vibrational modes in the FTIR spectra resembling graphene oxide.[42] This shows that the decomposition of $Ti_3C_2T_x$ MXene during hydrolysis results in a TiO_2/C composite that match well with previous reports on oxidation of $Ti_3C_2T_x$.[22,23,25] Apart from this oxidation, the MXene phase does not change much with the hydrolysation at lower temperatures. A slight shift in the (0 0 2) reflection upon increasing the hydrolysation can be seen in Figure S6a, which indicates a reduction in the interlayer spacing from 9.56 Å to 9.47 Å. Such changes in interlayer spacings are usually ascribed to deintercalation of H_2O from the MXene, but as the FTIR spectra do not give any indication of H_2O (Figure S7), and considering that each layer of water molecules is predicted to increase the spacing by > 2 Å,[11,43] dehydration is an unlikely explanation. Instead, the reduction in interlayer spacing upon hydrolysation might be ascribed to changes in the stacking of the MXene, as there are changes in intensity of the reflections between 33° and 45° upon hydrolysation, as well as a significant shift in the (1 1 0) reflection at 61° (Figure S6b).[44].

In Fig. 3a-d, the structural change of the MXene particles upon hydrolysation is presented through high-angle annular dark-field STEM (HAADF-STEM) micrographs. They show how the layered structure remains upon hydrolysation, although nanoparticles are formed after hydrolysation at 400 °C (Fig. 3c and Figure S8). Based on the results presented in Fig. 2, these nanoparticles are ascribed to TiO_2 (anatase). Although the macroscopic morphology of the MXene particles remains even after hydrolysation at 500 °C (Figure S8), the layered microstructure is no longer observed after complete oxidation. For the powders hydrolysed at 300 °C on the other hand, TiO_2 nanoparticles are not observed, which suggests insignificant oxidation by hydrolysation at this temperature. Additionally, an AB stacking of the pristine $Ti_3C_2T_x$ is demonstrated by the red lines in Fig. 3b,[45] which is similar to previously reported HAADF micrographs.[16,21] As the micrographs of the Hyd400C sample were viewed along the [1 0 0] zone axis (Fig. 3d), no more information about the MXene stacking could be obtained from these particles.

To measure the chemical compositional change in the bulk of the $Ti_3C_2T_x$ particles upon hydrolysation several SEM-EDS point scans from each sample were measured and the average results are presented in Fig. 3e. These values are presented relative to one formula unit of $Ti_3C_2T_x$ (per 3 Ti) and display how the O content increases with the oxidation of the MXene and ends up at twice the amount of Ti after hydrolysation at 500 °C, which again matches the formation of TiO_2. At the same time the C content remains roughly unchanged, demonstrating that H_2O is not sufficiently oxidising to form CO/CO_2 at these temperatures. When it comes to the removal of F terminations, hydrolysation seems to fail, as there are no significant changes in the F content after hydrolysation at 300 °C. The slight reduction at higher temperatures is

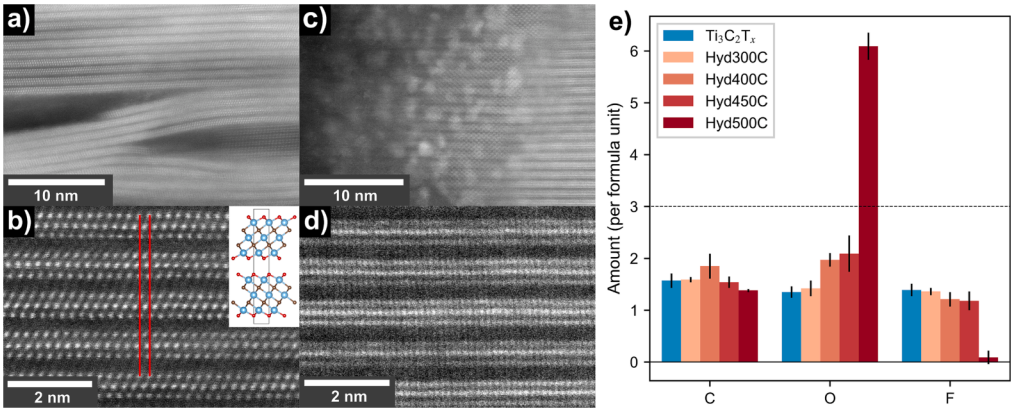

Fig. 3. HAADF-STEM images at two different magnifications of pristine $Ti_3C_2T_x$ MXene viewed along the [2 $\bar{1}$ 0] zone axis (a,b) and of $Ti_3C_2T_x$ after hydrolysation at 400 C viewed along the [1 0 0] zone axis (c,d), where the inset in (b) illustrates the AB stacking marked by the red lines. (e) shows the SEM EDS average values from point scans performed on pristine $Ti_3C_2T_x$ and $Ti_3C_2T_x$ hydrolysed at different temperatures, where the dashed line illustrates a Ti amount of 3 and the error bars represent the standard deviation from the set of point scans used for each sample. (For interpretation of the references to colour in this figure legend, the reader is referred to the web version of this article.)

likely related to the decompositionof the MXene phase, as the EDS results follow the same trends as the XRD, Raman and FTIR results presented in Fig. 2. As TEM EDS mapping of the edge surfaces demonstrated insignificant changes in local O and F concentrations before and after hydrolysation at 400 ℃ (Figure S9), it is concluded that the gas hydrolysation of pristine HF-etched $Ti_3C_2T_x$ does not result in any substitution of F-terminations.

Nonetheless, based on the oxidation products formed at elevated temperatures, gas hydrolysation still shows a higher selectivity towards F removal compared to other annealing atmospheres, as discussed further in the Supplementary Information (Figure S10-S14). Although annealing in dry synthetic air resulted in similar oxidation as the hydrolysation, it started at a lower temperature (300 ℃ for air and 400 ℃ for hydrolysis) and ended up with other products (Figure S10). While the annealing in dry air resulted in an oxidation of C to CO/CO_2 and the formation of a $TiOF_2$ phase, hydrolysation removed all F content while preserving most of the carbon content. Annealing in inert (Ar), reducing (H_2/Ar) and vacuum environments on the other hand, only resulted in minor oxidation to TiO_2 anatase (Figure S13 and S14) and insignificant compositional changes even after annealing at 500 ℃ (Table S1). These results are further discussed in the Supplementary Information. Noteworthy, the EDS mapping results show similar trends as the point scan averages (Table S2). Hence, use of EDS mapping may prove to be sufficient for rough quantification of O and F content for MXenes, if the number of impurity particles in the mapped regions are consistent.

3.3. *Hydrolysation of pre-intercalated $Ti_3C_2T_x$*

Considering the small interlayer spacing of the HF-etched $Ti_3C_2T_x$, which may have impeded the intercalation of H_2O molecules and thus also the hydrolysation reactions, pre-intercalation of various cations was attempted (denoted cation pillaring) to expand the interlayer spacing in the $Ti_3C_2T_x$ structure prior to hydrolysation. This cation pillaring was achieved by dispersing pristine $Ti_3C_2T_x$ powders in various hydroxide solutions to form $Ti_3C_2T_x$ intercalated with Li^+, Na^+, K^+, Mg^{2+} and tetrabutylammonium/TBA^+ (denoted "X-Ti_3C_2", where "X" represents the cation). As presented in the X-ray diffractograms in Fig. 4a, these pre-intercalations resulted in significant expansions of the interlayer spacings, from 9.56 Å in the pristine $Ti_3C_2T_x$, to around 12.4 Å for K-Ti_3C_2, Na-Ti_3C_2 and Li-Ti_3C_2, 14.8 Å for Mg-Ti_3C_2 and 17.4 Å for TBA-Ti_3C_2. Considering Mg-ions are shown to co-intercalate with two layers of water molecules at ambient conditions, whereas the alkali cations only co-intercalate with one layer, these results are in good agreement with previous reports.[46,47] However, after hydrolysing the pre-intercalated MXenes at 300 ℃ (X-Ti_3C_2-Hyd), the (0 0 2) reflections of the Li-Ti_3C_2, Mg-Ti_3C_2, and TBA-Ti_3C_2 samples are shifted back towards those of the pristine $Ti_3C_2T_x$, indicating a reduced interlayer spacing and hence a collapse of the pillared MXene structure. As the EDS results indicate insignificant changes in F content, it is assumed that the hydrolysation of these samples was unsuccessful due to the lack of H_2O intercalation. For the K-Ti_3C_2 and Na-Ti_3C_2 samples, however, the pillared MXene structures remained even after hydrolysation, which is demonstrated by the almost unchanged interlayer spacings (Fig. 4a). Unlike the non-pillared MXenes, the hydrolysation of these structures resulted in significant F reduction (45 % for Na-Ti_3C_2 and 64 % for K-Ti_3C_2 vs pristine $Ti_3C_2T_x$), accompanied by a comparable increase in O content (Fig. 4b). Seeing that these samples did not show any signs of oxidation (Figure S15–S18), these changes are ascribed to alterations in the mixture of termination groups. By extending the hydrolysation time of K-Ti_3C_2 from 15 h to 50 h an increased reduction of F content was achieved (78 % vs pristine $Ti_3C_2T_x$, Table S1), indicating an extensive removal of F terminations from the bulk of the $Ti_3C_2T_x$ particles upon hydrolysation. Furthermore, to ensure that the compositional changes were not related to the mere dehydration of the MXene, the K-Ti_3C_2 MXene was also annealed at 300 ℃ in dry Ar gas. Seeing that this resulted in insignificant changes in the F content (Table S1), the importance of water vapour to selectively remove F-terminations is demonstrated.

To ensure charge neutrality upon cation intercalation, all cations must have been co-intercalated with anions. Since hydroxide salts were used, it is likely that some OH-ions remain within the structure and assist the pillaring of the MXene. In the EDS data (Fig. 4b), this can be seen by the increase in the O content for all cation-intercalated samples compared to the pristine $Ti_3C_2T_x$. Strikingly, no Cl content was detected in the Mg-Ti_3C_2 samples after the cation substitution in $MgCl_2$ solutions (Table S1), implying that insignificant anion substitution has taken place. The increase in O content can also be partly ascribed to the

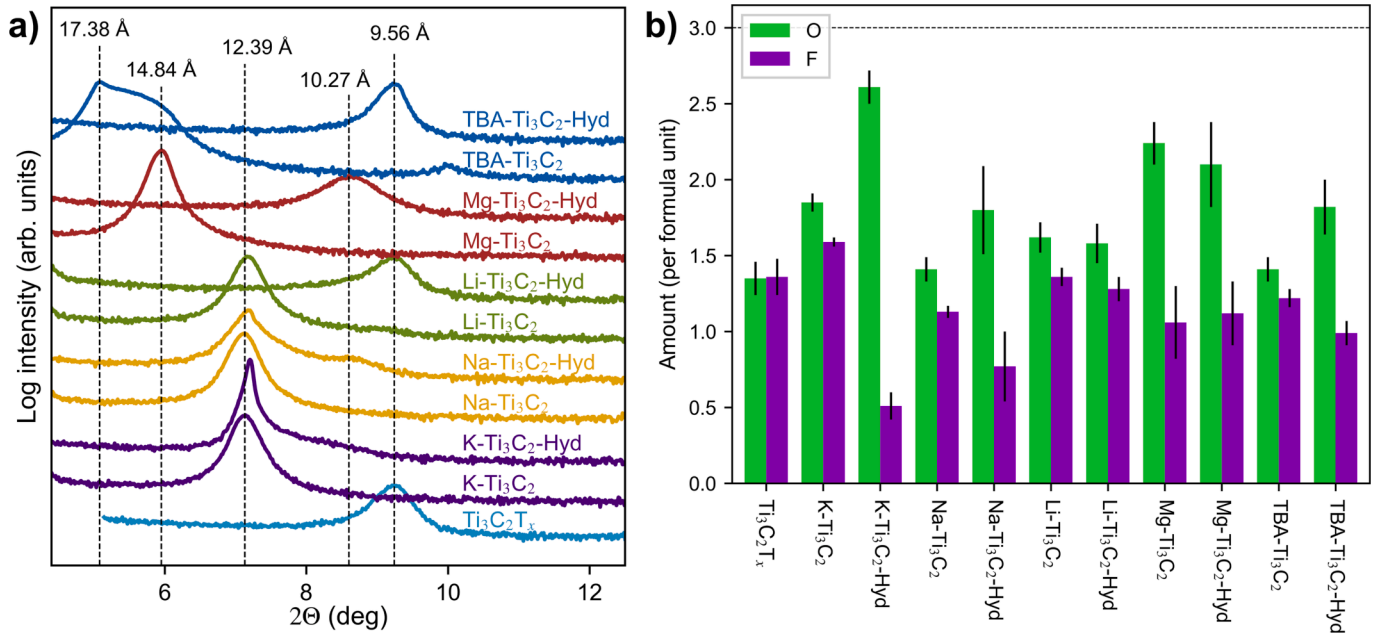

Fig. 4. Logarithmic intensities of low angle X-ray diffractograms (a) and EDS quantification of O and F (b) from the intercalation of various cations in $Ti_3C_2T_x$ followed by hydrolysation at 300 ℃. The dotted lines in (a) indicate the position of the (0 0 2) reflection for the different samples with the resulting interlayer spacings. The dashed line in (b) illustrates a Ti amount of 3 and the error bars represent the standard deviation from the set of point scans used for each sample.

intercalation of H_2O, which seems to match well with the higher interlayer spacing of Mg-Ti_3C_2. However, as the EDS data are acquired under high vacuum, it is difficult to know how much of the intercalated water remains within the structure during the measurements. The relative changes between F and O content on the other hand, is ascribed to changes in termination groups, and shows how the K-Ti_3C_2 and Na-Ti_3C_2 samples show the highest termination substitutions upon hydrolysation. However, from EDS data it is not possible to separate between O- and OH-terminations, leaving the exact mixture of the resulting termination groups after hydrolysation uncertain.

Apparent for all the pre-intercalated structures upon hydrolysation is a shift in the (0 0 2) reflection towards higher 2θ value and thereby also a smaller interlayer spacing. For the TBA-Ti_3C_2 sample it is likely that the TBA molecules decompose, as it matches well with the reduction in the C content (Table S1) and with previous reports on decomposition of intercalated TBA molecules by Ar annealing.[48,49] Similarly to the TBA-Ti_3C_2-Hyd, the interlayer spacing of Li-Ti_3C_2-Hyd is approximately the same as the pristine $Ti_3C_2T_x$. Surprisingly, this suggests a complete removal of the intercalated species upon hydrolysation, as intercalated Li-ions have been reported to result in up to a 20 % increase in interlayer spacing compared to the pristine MXene, both with and without the co-intercalation of solvents.[5,21,27] However, as the Li deintercalation is found to be very endothermic, it is possible that the slight increase in temperature is sufficient.[50] For the Mg-intercalated $Ti_3C_2T_x$ on the other hand, the reduction from 14.84 Å to around 10.3 Å upon hydrolysation is ascribed to the dehydration of water molecules, seeing that the Mg content remains unchanged (Table S1) and due to the removal of O—H vibrational modes in the FTIR spectra (Figure S15). As intercalated Mg-ions are calculated to have an ionic radius of 0.72 Å,[51] this correlates well with the difference in interlayer spacing from the pristine $Ti_3C_2T_x$. However, seeing that the cation intercalation must have been accompanied by intercalation of OH-ions for charge neutrality, there is also a possibility that the Mg-ions have bonded with residual OH-ions or with F-terminations to form insoluble $Mg(OH)_2$ and/or MgF_2 (Table S3).[13] Furthermore, a similar dehydration can be observed for Na-Ti_3C_2-Hyd, where a shoulder to the (0 0 2) reflection arises at around the same location as for Mg-Ti_3C_2-Hyd. This partial dehydration is also causing a general broadening of the XRD reflections with a non-zero l index in the Miller indices (*hkl*) after hydrolysation (Figure S16), as the interlayer spacing becomes less ordered. Although a small shoulder to the (0 0 2) reflection also appears after the hydrolysation of K-Ti_3C_2, the hydrolysation generally resulted in a sharpening of the reflections with $l \neq 0$ and thereby an increased ordering of the interlayer spacing. The minor shifts (0.12 Å) of the main (0 0 2) reflections in Na-Ti_3C_2 and K-Ti_3C_2 upon hydrolysation are almost identical, and may be ascribed to a small reduction in intercalated water.[43] However, as the reduction is < 5 % of one water layer,[43,47] the FTIR spectra in Figure S15 show no indications of H_2O, and according to previous reports claiming hydrophobic nature of these cations in MXenes,[51,52] this change might also be ascribed to changes in termination groups and stacking.[45] In Figure S17, a significant shift in the stacking sensitive (1 1 0) reflection can be seen after the hydrolysation of the K-intercalated MXene. Nonetheless, as the K-Ti_3C_2 sample maintained the best pillaring upon hydrolysation and the highest reduction of F content, it is reasonable to assume an essential role of the cation pillaring in the successful F removal by gas hydrolysation.

As demonstrated by the Raman and FTIR spectra in Fig. 5, the change in termination by hydrolysation also resulted in significant shifts in the vibrational modes of $Ti_3C_2T_x$. In the FTIR spectra, three vibrational modes are assigned to Ti-C and Ti-T modes (T = termination group) at 575 cm^{-1} and 650 cm^{-1} for the pristine $Ti_3C_2T_x$, respectively, as well as K-T modes at around 955 cm^{-1}. Upon intercalation of K-ions, the Ti-related modes do not shift significantly. However, upon hydrolysation of K-Ti_3C_2, the Ti-T and Ti-C modes are shifted by 20–50 cm^{-1} to higher wavenumbers, which is ascribed to a reduced amount of F-terminations.[53] Similarly, the K-T vibration is shifted slightly down, which also match with the change in terminations. Additionally, in the Raman spectra in Fig. 5b, there are significant shifts in the out-of-plane A_{1g} (C) peak at 717 cm^{-1} upon both K-intercalation and hydrolysation, corresponding to an increased interlayer spacing as well as the reduction of F-terminations.[33] In addition, there are significant shifts in the in-plane E_g peaks at around 209 cm^{-1}, 380 cm^{-1} and 610 cm^{-1}, and small shifts in the A_{1g} peak at 209 cm^{-1} and the resonant peak at 121 cm^{-1}, which also match with the expected changes for increased amounts of O-terminations.[33,54] Although these peak shifts indicate more O-terminations, matching the DFT predictions presented in Fig. 1, it is not possible to obtain any useful information about the exact ratio between O- and OH-terminations after hydrolysation from these results. To better quantify this termination ratio in bulk powders, one would need to use methods such as ^{1}H NMR,[9] neutron scattering,[55] or XPS depth profiling.[56].

Furthermore, an interesting aspect with the hydrolysation of the cation pillared MXenes is the trend of which cations were able to hold the intercalated water upon hydrolysation. Based on the hydration enthalpies presented in Table S3, one would assume the opposite results, as Mg-ions have the highest hydration enthalpy of the four cations (Mg^{2+}, Li^+, Na^+ and K^+), and therefore would be expected to hold the surrounding water molecules the strongest. Although previous reports

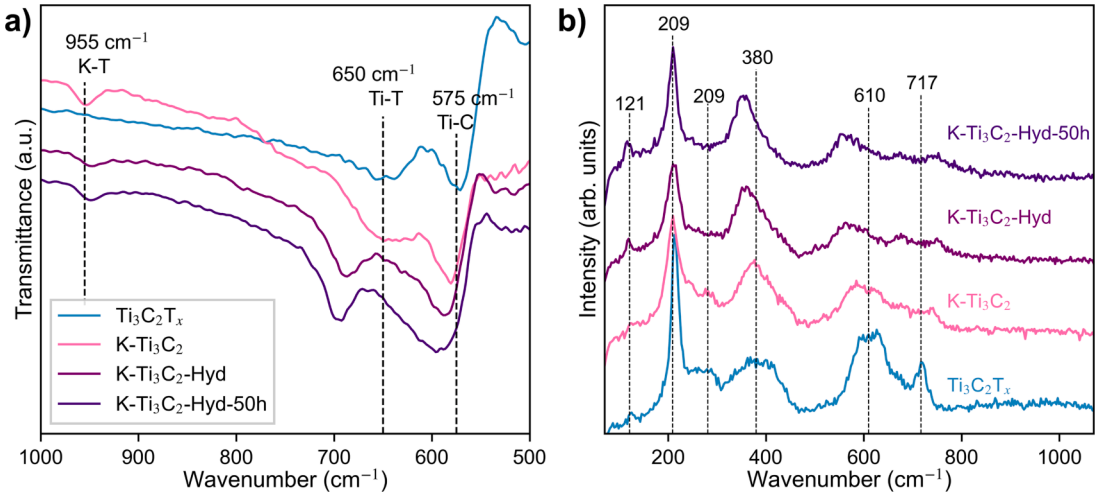

Fig. 5. FTIR (a) and Raman (b) spectra of $Ti_3C_2T_x$ and K-Ti_3C_2 before and after hydrolysation at 300 ℃ for 15 h and 50 h. The dotted lines in both spectra are used to indicate the location of the vibrational modes for the pristine $Ti_3C_2T_x$ and thus illustrate the shifts that occur upon intercalation of K-ions and after hydrolysation.

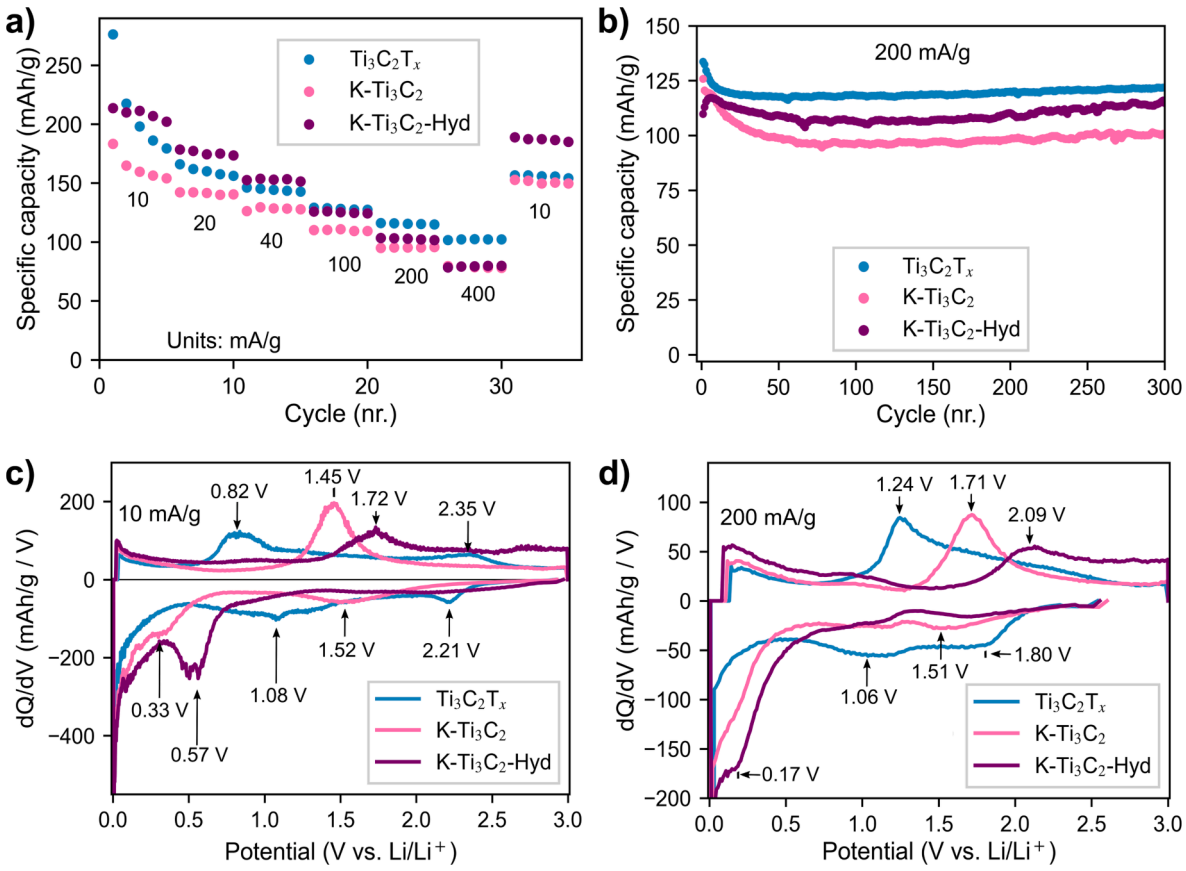

Fig. 6. Electrochemical evaluation of $Ti_3C_2T_x$, K-Ti_3C_2 and K-Ti_3C_2-Hyd electrodes in LiB half cells, showing specific delithiation capacities per cycle at various specific currents (a), and for long term cycling at 200 mA/g (b). Corresponding differential capacity profiles at 10 mA/g (c) and 200 mA/g (d) are from cycle 3 and 23 presented in (a), respectively.

suggest a clay-like behaviour of MXenes with 1–2 layers of water molecules following the intercalation of cations,[43,57–59] there are also reports suggesting that larger cations such as K would even extract water from the MXenes upon intercalation.[51] Based on the lack of H_2O vibrations in the FTIR spectra of K-Ti_3C_2, it is possible that the K-, Na- and Li-intercalated samples encompass zero layers of water molecules. However, due to the similarity of the interlayer spacings for all these cations and the calculated size of one layer of water molecules, the presence of intercalated water is very likely. Instead, the dehydration of the MXenes can most likely be attributed to the diffusion of intercalated water, where the diffusion coefficient is larger for the smaller cations.[43,59] This implies that although K-ions have the lowest hydration enthalpy, they have the strongest ability to prevent water molecules from leaving the interlayers of the MXene upon increasing the temperature. In fact, by hydrolysation at 300 ℃, the thermal energy may even be high enough to dehydrate all the different cations regardless of the hydration enthalpy. Additionally, it should be highlighted that the amount of co-intercalated water seems to strongly affect the stacking faults in the $Ti_3C_2T_x$ layers. While all the cation-intercalated structures with one water layer (K-Ti_3C_2, Na-$Ti_3C_2$and Li-Ti_3C_2) shows significantly more defined reflections in the 35-45° region compared to the pristine $Ti_3C_2T_x$, the Mg-Ti_3C_2 sample with two layers of water molecules does not.[44].

3.4. *Electrochemical evaluation of hydrolysed K-intercalated $Ti_3C_2T_x$*

As the hydrolysation of K-Ti_3C_2 resulted in the greatest F reduction, the electrochemical performance of $Ti_3C_2T_x$, K-Ti_3C_2 and K-Ti_3C_2-Hyd electrodes was evaluated by galvanostatic charge and discharge cycling in LiB half cells. Capacity plots from tests at various current densities are presented in Fig. 6a and b and they demonstrate how intercalation of K-ions resulted in a significant capacity reduction, both at low and high current densities. A similar capacity reduction upon K-intercalation has been reported for Na-ion batteries,[52] and may be ascribed to the K-ions blocking some of the possible intercalation sites for Li-ions upon cycling. With an approximated ~ 10 % K occupation of the intercalation sites inside the MXene (Table S1), and considering the possible blocking by the co-intercalated OH-ions, the reduction of around 20 % is to be expected. However, for the hydrolysed sample the capacity is increased, which can be ascribed to a reduced amount of F and OH-terminations that are assumed to either sterically hinder some Li-ion intercalation or end up with the formation of LiF or LiOH side products.[11,12] Seeing that the pristine $Ti_3C_2T_x$ and K-Ti_3C_2 electrodes show a significant capacity fade upon the first cycles, it is possible that the hydrolysed sample results in the formation of less side products during cycling, which again enables capacities closer to the theoretical limit of 268 mAh/g for $Ti_3C_2O_2Li_2$.[11,60] At lower current densities, the delithiation capacities obtained with K-Ti_3C_2-Hyd electrodes are higher than the pristine $Ti_3C_2T_x$, with 187 mAh/g vs 156 mAh/g at cycle 33 (Fig. 6a), even though all of the intercalated K-ions remained after hydrolysis (Table S1). At higher current densities on the other hand, the capacity fades quickly and at current densities > 40 mA/g the capacity of the pristine $Ti_3C_2T_x$ is higher. This capacity reduction at higher current densities may partly be ascribed to K-ions slowing the Li-migration, as a similar trend is also observed for the K-Ti_3C_2 sample. However, as the capacity reduction in the hydrolysed sample is significantly higher, it is also possible that the change in termination groups has an effect. Interestingly, DFT calculations predict lower migration barriers for Li-ions on O-terminated surfaces compared to F- and OH-terminated ones,[11,12] which should have resulted in better rate performance. However, they also demonstrate how the stacking of the MXene sheets

greatly influence the migration barriers.[61] As the K-Ti_3C_2-Hyd sample demonstrated a significant shift in the (0 0 1) reflection and thus a possible change in stacking (Figure S17), it is possible that the lesser rate capability of this material may be ascribed to stacking changes.

The intercalation of K-ions and the following hydrolysation also affected the intercalation voltages during cycling, which is illustrated by the differential capacity plots in Fig. 6c and d. From the low current density (10 mA/g) plot in Fig. 6c, it is shown how the intercalation of K-ions lowered the voltage of the lithiation peaks from 2.21 V and 1.58 V in $Ti_3C_2T_x$ to 1.52 V and 0.33 V, while the hydrolysation resulted in a shift of the biggest lithiation peak from 0.33 V to 0.57 V while flattening out the peak at 1.52 V. This shows that the intercalation of K-ions significantly lower the intercalation voltage of Li-ions, and that the removal of F-terminations by hydrolysation causes a slight increase in intercalation voltage, matching well with more O-terminations being formed.[11–13] However, upon delithiation the peaks of the K-intercalated electrodes are moved to higher voltages, indicating a significant energy inefficiency compared to the pristine $Ti_3C_2T_x$. At higher current densities (Fig. 6d), an even higher overpotential is observed for the K-intercalated electrodes, as the main lithiation peaks are shifted down to below 0.3 V, while the main delithiation peaks are shifted to 1.71 V and 2.09 V for K-Ti_3C_2 and K-Ti_3C_2-Hyd, respectively. The pristine $Ti_3C_2T_x$ on the other hand, retains most of the lithiation and delithiation capacities between 1 V and 2 V, which is similar to what has been reported previously.[5,62] Although these results demonstrate how the change in terminations can alter the electrochemical performance of $Ti_3C_2T_x$ MXene for LiBs, the negative effect of the K-ion intercalation still limits the feasibility of gas hydrolysation to improve the Li-intercalating properties of the MXene. To improve the LiB performance after gas hydrolysation of $Ti_3C_2T_x$, K-ion intercalation should somehow be bypassed. Either by pillaring the MXene with other cations, or by removing or substituting the K-ions after the hydrolysation is completed. Additionally, it should be noted that to the authors' knowledge, this is the first report on Li-intercalation in K pre-intercalated MXenes. Seeing that the K-ions may block some of the Li-intercalation sites, the K-intercalated $Ti_3C_2T_x$ may be more suitable for other battery chemistries. In fact, for aqueous supercapacitors Prenger et al. recently demonstrated a 10-fold areal capacitance increase of multilayered $Ti_3C_2T_x$ compared to delaminated films, by pre-intercalation of the same cations as presented here (Mg^{2+}, Li^+, Na^+ and K^+).[63] They also showed how the K-intercalated $Ti_3C_2T_x$ phase resulted in the highest capacitance of all these cation-intercalated structures, which indicates how further investigation on this K-Ti_3C_2 phase also could be highly relevant for other applications.

4. Conclusion

Gas hydrolysation has been investigated as a method to substitute F-terminations with O- and OH-terminations on the 2D surfaces of $Ti_3C_2T_x$ MXene, together with a comparison of the thermal stability of this phase in various atmospheres. Pristine HF-etched $Ti_3C_2T_x$ MXene is found to remain stable up to a temperature of 300 ℃, after which it starts to oxidise into TiO_2 nanoparticles and disordered graphitic carbon. Oxidation starts on the edge surfaces of the particles, but after hydrolysation at 500 ℃ the MXene phase is completely transformed to a TiO_2/C composite. The oxidation of $Ti_3C_2T_x$ in humid inert atmosphere starts at a higher temperature (~400 ℃) than in dry air (~300 ℃). Compared to air annealing, hydrolysation also demonstrates a higher selectivity towards F removal. While the 500 ℃ annealing in dry air resulted in an oxidation of C to CO_2 and the formation of a $TiOF_2$ phase, hydrolysation at 500 ℃ removed almost all F content while preserving most of the carbon content. However, as the water molecules were unable to penetrate the pristine MXene structure, the hydrolysation resulted in no reduction of F-terminations prior to the decomposition.

We have shown that successful substitution of F-terminations from multilayered $Ti_3C_2T_x$ particles requires a pillaring of the structure to allow for H_2O intercalation between the 2D layers. This was demonstrated by pre-intercalating $Ti_3C_2T_x$ with various cations (Li^+, Na^+, K^+, Mg^{2+}, TBA^+) together with 1–2 layers of H_2O molecules, which resulted in 2.8–7.8 Å increase in the interlayer spacing. Upon hydrolysation at 300 ℃, three of the samples (Li-Ti_3C_2, Mg-Ti_3C_2 and TBA-Ti_3C_2) collapsed and ended up with an interlayer spacing matching the pristine HF-etched $Ti_3C_2T_x$ (~9.7 Å), together with insignificant changes in F content. However, for the K-Ti_3C_2 and Na-Ti_3C_2 samples the pillaring structure remained after hydrolysation, which resulted in a significant reduction in F-terminations (45 % for Na-Ti_3C_2 and 64 % for K-Ti_3C_2 vs pristine $Ti_3C_2T_x$) along with a similar increase in O content. By extending the hydrolysation time to 50 h, a total F reduction of 78 % was achieved, without any signs of surface oxidation. In addition, the fundamental role of H_2O vapour upon hydrolysation was proven by the insignificant F change upon annealing of the K-Ti_3C_2 sample in dry Ar gas. Cation intercalation followed by gas hydrolysation is thus proposed as a new method to substitute significant amounts of F-terminations from the bulk of $Ti_3C_2T_x$ particles.

Moreover, the electrochemical performance of K-intercalated $Ti_3C_2T_x$ before and after changing the termination groups by hydrolysation has been evaluated. Firstly, the K-intercalated electrodes demonstrated significantly worse energy efficiency compared to the pristine $Ti_3C_2T_x$, which was ascribed to steric hindrance. The intercalation of K-ions also reduced the specific capacity by blocking Li sites upon cycling. Hydrolysation of the MXene on the other hand, resulted in a slight increase in reversible capacity, which was ascribed to less irreversible reactions with F- and OH-terminations. Additionally, it resulted in increased (de)intercalation voltages and thereby demonstrate gas hydrolysation as a feasible method to control the electrochemical performance of $Ti_3C_2T_x$ electrodes in LiBs.

CRediT authorship contribution statement

Frode Håskjold Fagerli: Investigation, Formal analysis, Writing – original draft. **Per Erik Vullum:** Investigation, Writing – review & editing. **Tor Grande:** Conceptualization, Writing – review & editing. **Zhaohui Wang:** Software, Writing – review & editing. **Sverre M. Selbach:** Writing – review & editing. **Kjell Wiik:** Supervision, Writing – review & editing. **Nils Peter Wagner:** Supervision, Writing – review & editing.

Declaration of Competing Interest

The authors declare that they have no known competing financial interests or personal relationships that could have appeared to influence the work reported in this paper.

Data availability

Data will be made available on request.

Acknowledgements

This work was financially supported by the Research Council of Norway through the project "High-capacity 2D layered materials for Mg-ion batteries" (project number 275810). The computational resources were provided by UNINETT Sigma2 through the project NN9264K. The TEM work was carried out on NORTEM infrastructure, Grant 197405, TEM Gemini Centre, Norwegian University of Science and Technology (NTNU), Norway. The Research Council of Norway is acknowledged for the support to the Norwegian Micro- and Nano-Fabrication Facility, NorFab, project number 295864. Additionally, the authors would like to thank Prof. Andreas Erbe for his guidance in the interpretation of the FTIR spectra, and Dr. Henning Kaland for useful discussions in the early stages of this work.

Appendix A. Supplementary data

Supplementary data to this article can be found online at https://doi.org/10.1016/j.flatc.2023.100470.

References

[1] F. Shahzad, M. Alhabeb, C.B. Hatter, B. Anasori, S. Man Hong, C.M. Koo, Y. Gogotsi, Electromagnetic interference shielding with 2D transition metal carbides (MXenes), Science 353 (6304) (2016) 1137–1140.

[2] Y. Cai, J. Shen, C.W. Yang, Y. Wan, H.L. Tang, A.A. Aljarb, C. Chen, J.H. Fu, X. Wei, K.W. Huang, Y. Han, S.J. Jonas, X. Dong, V. Tung, Mixed-dimensional MXene-hydrogel heterostructures for electronic skin sensors with ultrabroad working range, Sci. Adv. 6 (2020) 5367–5394, https://doi.org/10.1126/sciadv.abb5367.

[3] Y.A.J. Al-Hamadani, B.M. Jun, M. Yoon, N. Taheri-Qazvini, S.A. Snyder, M. Jang, J. Heo, Y. Yoon, Applications of MXene-based membranes in water purification: A review, Chemosphere. 254 (2020), 126821, https://doi.org/10.1016/J.CHEMOSPHERE.2020.126821.

[4] K. Huang, Z. Li, J. Lin, G. Han, P. Huang, Two-dimensional transition metal carbides and nitrides (MXenes) for biomedical applications, Chem. Soc. Rev. 47 (2018) 5109–5124, https://doi.org/10.1039/c7cs00838d.

[5] M. Naguib, J. Come, B. Dyatkin, V. Presser, P.-L. Taberna, P. Simon, M. W. Barsoum, Y. Gogotsi, MXene: a promising transition metal carbide anode for lithium-ion batteries, Electrochem. Commun. 16 (2012) 61–64, https://doi.org/10.1016/J.ELECOM.2012.01.002.

[6] R. Garg, A. Agarwal, M. Agarwal, A review on MXene for energy storage application: effect of interlayer distance, Mater. Res. Express. 7 (2020) 022001. https://doi.org/10.1088/2053-1591/AB750D.

[7] M. Hu, H. Zhang, T. Hu, B. Fan, X. Wang, Z. Li, Emerging 2D MXenes for supercapacitors: status, challenges and prospects, Chem. Soc. Rev. 49 (2020) 6666–6693, https://doi.org/10.1039/D0CS00175A.

[8] A. VahidMohammadi, J. Rosen, Y. Gogotsi, The world of two-dimensional carbides and nitrides (MXenes), Science. 372 (2021), https://doi.org/10.1126/SCIENCE.ABF1581.

[9] M.A. Hope, A.C. Forse, K.J. Griffith, M.R. Lukatskaya, M. Ghidiu, Y. Gogotsi, C. P. Grey, NMR reveals the surface functionalisation of Ti_3C_2 MXene, Phys. Chem. Chem. Phys. 18 (2016) 5099–5102, https://doi.org/10.1039/C6CP00330C.

[10] M. Naguib, V.N. Mochalin, M.W. Barsoum, Y. Gogotsi, 25th anniversary article: MXenes: A new family of two-dimensional materials, Adv. Mater. 26 (2014) 992–1005, https://doi.org/10.1002/adma.201304138.

[11] Y. Xie, M. Naguib, V.N. Mochalin, M.W. Barsoum, Y. Gogotsi, X. Yu, K.-W. Nam, X.-Q. Yang, A.I. Kolesnikov, P.R.C. Kent, Role of Surface Structure on Li-Ion Energy Storage Capacity of Two-Dimensional Transition-Metal Carbides, J. Am. Chem. Soc. 136 (2014) 6385–6394, https://doi.org/10.1021/ja501520b.

[12] Q. Tang, Z. Zhou, P. Shen, Are MXenes promising anode materials for Li ion batteries? Computational studies on electronic properties and Li storage capability of Ti_3C_2 and $Ti_3C_2X_2$ (X = F, OH) monolayer, J. Am. Chem. Soc. 134 (2012) 16909–16916, https://doi.org/10.1021/JA308463R.

[13] H. Kaland, J. Hadler-Jacobsen, F.H. Fagerli, N.P. Wagner, Z. Wang, S.M. Selbach, F. Vullum-Bruer, K. Wiik, S.K. Schnell, Are MXenes suitable as cathode materials for rechargeable Mg batteries?, Sustain, Energy Fuels. 4 (2020) 2956–2966, https://doi.org/10.1039/D0SE00087F.

[14] C. Eames, M.S. Islam, Ion intercalation into two-dimensional transition-metal carbides: Global screening for new high-capacity battery materials, J. Am. Chem. Soc. 136 (2014) 16270–16276, https://doi.org/10.1021/ja508154e.

[15] Z. Bao, C. Lu, X. Cao, P. Zhang, L. Yang, H. Zhang, D. Sha, W. He, W. Zhang, L. Pan, Z. Sun, Role of MXene surface terminations in electrochemical energy storage: A review, Chinese Chem. Lett. 32 (2021) 2648–2658, https://doi.org/10.1016/J.CCLET.2021.02.012.

[16] V. Kamysbayev, A.S. Filatov, H. Hu, X. Rui, F. Lagunas, D.i. Wang, R.F. Klie, D. V. Talapin, Covalent surface modifications and superconductivity of two-dimensional metal carbide MXenes, Science 369 (6506) (2020) 979–983.

[17] L. Huang, T. Li, Q. Liu, J. Gu, Fluorine-free $Ti_3C_2T_x$ as anode materials for Li-ion batteries, Electrochem. Commun. 104 (2019), 106472, https://doi.org/10.1016/j.elecom.2019.05.021.

[18] Y. Li, H. Shao, Z. Lin, J. Lu, L. Liu, B. Duployer, P.O.Å. Persson, P. Eklund, L. Hultman, M. Li, K.e. Chen, X.-H. Zha, S. Du, P. Rozier, Z. Chai, E. Raymundo-Piñero, P.-L. Taberna, P. Simon, Q. Huang, A general Lewis acidic etching route for preparing MXenes with enhanced electrochemical performance in non-aqueous electrolyte, Nat. Mater. 19 (8) (2020) 894–899.

[19] R.A. Vaia, A. Jawaid, A. Hassan, G. Neher, D. Nepal, R. Pachter, W. Joshua Kennedy, S. Ramakrishnan, Halogen etch of Ti_3AlC_2 MAX phase for MXene fabrication, ACS Nano. 15 (2021) 2771–2777, https://doi.org/10.1021/ACSNANO.0C08630.

[20] Z. Li, L. Wang, D. Sun, Y. Zhang, B. Liu, Q. Hu, A. Zhou, Synthesis and thermal stability of two-dimensional carbide MXene Ti_3C_2, Mater. Sci. Eng. B Solid-State Mater. Adv. Technol. 191 (2015) 33–40, https://doi.org/10.1016/j.mseb.2014.10.009.

[21] R. Cheng, T. Hu, H. Zhang, C. Wang, M. Hu, J. Yang, C. Cui, T. Guang, C. Li, C. Shi, P. Hou, X. Wang, Understanding the Lithium Storage Mechanism of $Ti_3C_2T_x$ MXene, J. Phys. Chem. C. 123 (2) (2019) 1099–1109.

[22] S. Doo, A. Chae, D. Kim, T. Oh, T.Y. Ko, S.J. Kim, D.Y. Koh, C.M. Koo, Mechanism and Kinetics of Oxidation Reaction of Aqueous $Ti_3C_2T_x$ Suspensions at Different pHs and Temperatures, ACS Appl. Mater. Interfaces. 13 (2021) 22855–22865, https://doi.org/10.1021/ACSAMI.1C04663.

[23] X. Zhang, Y. Liu, S. Dong, Z. Ye, Y. Guo, One-step hydrothermal synthesis of a TiO_2-$Ti_3C_2T_x$ nanocomposite with small sized TiO_2 nanoparticles, Ceram. Int. 43 (2017) 11065–11070, https://doi.org/10.1016/J.CERAMINT.2017.05.151.

[24] J. Halim, I. Persson, P. Eklund, P.O.Å. Persson, J. Rosen, Sodium hydroxide and vacuum annealing modifications of the surface terminations of a Ti_3C_2 (MXene) epitaxial thin film, RSC Adv. 8 (2018) 36785–36790, https://doi.org/10.1039/c8ra07270a.

[25] M. Naguib, O. Mashtalir, M.R. Lukatskaya, B. Dyatkin, C. Zhang, V. Presser, Y. Gogotsi, M.W. Barsoum, One-step synthesis of nanocrystalline transition metal oxides on thin sheets of disordered graphitic carbon by oxidation of MXenes, Chem. Commun. 50 (2014) 7420–7423, https://doi.org/10.1039/c4cc01646g.

[26] I. Persson, J. Halim, T.W. Hansen, J.B. Wagner, V. Darakchieva, J. Palisaitis, J. Rosen, P.O.Å. Persson, How Much Oxygen Can a MXene Surface Take Before It Breaks? Adv. Funct. Mater. 30 (47) (2020) 1909005.

[27] P. Bärmann, R. Nölle, V. Siozios, M. Ruttert, O. Guillon, M. Winter, J. Gonzalez-Julian, T. Placke, Solvent Co-intercalation into Few-layered $Ti_3C_2T_x$ MXenes in Lithium Ion Batteries Induced by Acidic or Basic Post-treatment, ACS Nano. 15 (2) (2021) 3295–3308.

[28] J. Li, X. Yuan, C. Lin, Y. Yang, L. Xu, X. Du, J. Xie, J. Lin, J. Sun, J. Li, X. Yuan, C. Lin, Y. Yang, L. Xu, X. Du, J. Xie, J. Lin, J. Sun, Achieving High Pseudocapacitance of 2D Titanium Carbide (MXene) by Cation Intercalation and Surface Modification, Adv. Energy Mater. 7 (2017) 1602725, https://doi.org/10.1002/AENM.201602725.

[29] J. Zhao, J. Wen, J. Xiao, X. Ma, J. Gao, L. Bai, H. Gao, X. Zhang, Z. Zhang, Nb_2CT_x MXene: High capacity and ultra-long cycle capability for lithium-ion battery by regulation of functional groups, J. Energy Chem. 53 (2021) 387–395, https://doi.org/10.1016/J.JECHEM.2020.05.037.

[30] F.H. Fagerli, Z. Wang, T. Grande, H. Kaland, S.M. Selbach, N.P. Wagner, K. Wiik, Removing Fluoride-Terminations from Multilayered V_2CT_x MXene by Gas Hydrolyzation, ACS Omega. 7 (2022) 23790–23799, https://doi.org/10.1021/acsomega.2c02441.

[31] F.A. Lukiyanov, E.I. Rau, R.A. Sennov, Depth range of primary electrons, electron beam broadening, and spatial resolution in electron-beam studies, Bull. Russ. Acad. Sci. Phys. 73 (4) (2009) 441–449.

[32] A. Wexler, Vapor pressure formulation for water in range 0 to 100 Degrees C. A revision, accessed July 2, 2022, J. Res. Natl. Bur. Stand. - A. Phys. Chem. 80A (1976) 775–785, https://nvlpubs.nist.gov/nistpubs/jres/80A/jresv80An5-6p775_A1b.pdf.

[33] A. Sarycheva, Y. Gogotsi, Raman Spectroscopy Analysis of the Structure and Surface Chemistry of $Ti_3C_2T_x$ MXene, Chem. Mater. 32 (2020) 3480–3488, https://doi.org/10.1021/acs.chemmater.0c00359.

[34] G. Kresse, D. Joubert, From ultrasoft pseudopotentials to the projector augmented-wave method, Phys. Rev. B. 59 (3) (1999) 1758–1775.

[35] P.E. Blöchl, Projector augmented-wave method, Phys. Rev. B. 50 (24) (1994) 17953–17979.

[36] G. Kresse, J. Furthmüller, Efficient iterative schemes for *ab initio* total-energy calculations using a plane-wave basis set, Phys. Rev. B. 54 (16) (1996) 11169–11186.

[37] K.J. Atkins, P. W., de Paula J.,, Physical Chemistry, 11th ed,, Oxford Univ. Press, Oxford, 2017, p. 944.

[38] A. Togo, I. Tanaka, First principles phonon calculations in materials science, Scr. Mater. 108 (2015) 1–5, https://doi.org/10.1016/J.SCRIPTAMAT.2015.07.021.

[39] D. Russell, Johnson, NIST Computational Chemistry Comparison and Benchmark Database, NIST Stand. Ref. Database Number 101 (2022). https://doi.org/10.18434/T47C7Z.

[40] F. Destyorini, Y. Irmawati, A. Hardiansyah, H. Widodo, I.N.D. Yahya, N. Indayaningsih, R. Yudianti, Y.I. Hsu, H. Uyama, Formation of nanostructured graphitic carbon from coconut waste via low-temperature catalytic graphitisation, Eng. Sci. Technol. an Int. J. 24 (2021) 514–523, https://doi.org/10.1016/J.JESTCH.2020.06.011.

[41] P.K. Chu, L. Li, Characterization of amorphous and nanocrystalline carbon films, Mater. Chem. Phys. 96 (2006) 253–277, https://doi.org/10.1016/J.MATCHEMPHYS.2005.07.048.

[42] R.A. Rochman, S. Wahyuningsih, A.H. Ramelan, Q.A. Hanif, Preparation of nitrogen and sulphur Co-doped reduced graphene oxide (rGO-NS) using N and S heteroatom ofthiourea, IOP Conf. Ser. Mater. Sci. Eng. 509 (2019), 012119, https://doi.org/10.1088/1757-899X/509/1/012119.

[43] N.C. Osti, M. Naguib, A. Ostadhossein, Y. Xie, P.R.C. Kent, B. Dyatkin, G. Rother, W.T. Heller, A.C.T. Van Duin, Y. Gogotsi, E. Mamontov, Effect of Metal Ion Intercalation on the Structure of MXene and Water Dynamics on its Internal Surfaces, ACS Appl. Mater. Interfaces. 8 (2016) 8859–8863, https://doi.org/10.1021/acsami.6b01490.

[44] C. Ferrara, A. Gentile, S. Marchionna, I. Quinzeni, M. Fracchia, P. Ghigna, S. Pollastri, C. Ritter, G.M. Vanacore, R. Ruffo, The Missing Piece: The Structure of the $Ti_3C_2T_x$ MXene and Its Behavior as Negative Electrode in Sodium Ion Batteries, Nano Lett. 21 (2021) 8290–8297, https://doi.org/10.1021/ACS.NANOLETT.1C02809.

[45] J. Hadler-Jacobsen, F.H. Fagerli, H. Kaland, S.K. Schnell, Stacking Sequence, Interlayer Bonding, Termination Group Stability and Li/Na/Mg Diffusion in MXenes, ACS Mater. Lett. 3 (2021) 1369–1376, https://doi.org/10.1021/ACSMATERIALSLETT.1C00316.

[46] P. Yu, G. Cao, S. Yi, X. Zhang, C. Li, X. Sun, K. Wang, Y. Ma, Binder-free 2D titanium carbide (MXene)/carbon nanotube composites for high-performance

lithium-ion capacitors, Nanoscale. 10 (2018) 5906–5913, https://doi.org/10.1039/C8NR00380G.
[47] M. Ghidiu, J. Halim, S. Kota, D. Bish, Y. Gogotsi, M.W. Barsoum, Ion-Exchange and Cation Solvation Reactions in Ti_3C_2 MXene, Chem. Mater. 28 (2016) 3507–3514, https://doi.org/10.1021/acs.chemmater.6b01275.
[48] J.L. Hart, K. Hantanasirisakul, A.C. Lang, B. Anasori, D. Pinto, Y. Pivak, J.T. van Omme, S.J. May, Y. Gogotsi, M.L. Taheri, Control of MXenes' electronic properties through termination and intercalation, Nat. Commun. 10 (2019) 522, https://doi.org/10.1038/s41467-018-08169-8.
[49] Y. Xia, L. Que, F. Yu, L. Deng, Z. Liang, Y. Jiang, M. Sun, L. Zhao, Z. Wang, Tailoring Nitrogen Terminals on MXene Enables Fast Charging and Stable Cycling Na-Ion Batteries at Low Temperature, Nano-Micro Lett. 14 (1) (2022).
[50] G. Sharma, E. Muthuswamy, M. Naguib, Y. Gogotsi, A. Navrotsky, D. Wu, Calorimetric Study of Alkali Metal Ion (K+, Na+, Li+) Exchange in a Clay-Like MXene, J. Phys. Chem. C. 121 (2017) 15145–15153, https://doi.org/10.1021/ACS.JPCC.7B02419.
[51] N. Shpigel, M.D. Levi, S. Sigalov, T.S. Mathis, Y. Gogotsi, D. Aurbach, Direct Assessment of Nanoconfined Water in 2D Ti_3C_2 Electrode Interspaces by a Surface Acoustic Technique, J. Am. Chem. Soc. 140 (2018) 8910–8917, https://doi.org/10.1021/JACS.8B04862.
[52] J. Luo, C. Fang, C. Jin, H. Yuan, O. Sheng, R. Fang, W. Zhang, H. Huang, Y. Gan, Y. Xia, C. Liang, J. Zhang, W. Li, X. Tao, Tunable pseudocapacitance storage of MXene by cation pillaring for high performance sodium-ion capacitors, J. Mater. Chem. A. 6 (2018) 7794–7806, https://doi.org/10.1039/C8TA02068J.
[53] H.u. Tao, J. Wang, H. Zhang, Z. Li, H.u. Minmin, X. Wang, Vibrational properties of Ti_3C_2 and $Ti_3C_2T_2$ (T = O, F, OH) monosheets by first-principles calculations: a comparative study, Phys. Chem. Chem. Phys. 17 (2015) 9997–10003, https://doi.org/10.1039/C4CP05666C.
[54] H. Li, S. Chen, D.W. Boukhvalov, Z. Yu, M.G. Humphrey, Z. Huang, C. Zhang, Switching the Nonlinear Optical Absorption of Titanium Carbide MXene by Modulation of the Surface Terminations, ACS Nano. 16 (1) (2022) 394–404.
[55] H.W. Wang, M. Naguib, K. Page, D.J. Wesolowski, Y. Gogotsi, Resolving the Structure of $Ti_3C_2T_x$ MXenes through Multilevel Structural Modeling of the Atomic Pair Distribution Function, Chem. Mater. 28 (2016) 349–359, https://doi.org/10.1021/acs.chemmater.5b04250.
[56] J. Halim, K.M. Cook, M. Naguib, P. Eklund, Y. Gogotsi, J. Rosen, M.W. Barsoum, X-ray photoelectron spectroscopy of select multi-layered transition metal carbides (MXenes), Appl. Surf. Sci. 362 (2016) 406–417, https://doi.org/10.1016/J.APSUSC.2015.11.089.
[57] N.C. Osti, M. Naguib, K. Ganeshan, Y.K. Shin, A. Ostadhossein, A.C.T. Van Duin, Y. Cheng, L.L. Daemen, Y. Gogotsi, E. Mamontov, A.I. Kolesnikov, Influence of metal ions intercalation on the vibrational dynamics of water confined between MXene layers, Phys. Rev. Mater. 1 (2017), 065406, https://doi.org/10.1103/PHYSREVMATERIALS.1.065406/FIGURES/5/MEDIUM.
[58] M.R. Lukatskaya, O. Mashtalir, C.E. Ren, Y. Dall'Agnese, P. Rozier, P.L. Taberna, M. Naguib, P. Simon, M.W. Barsoum, Y. Gogotsi, Cation intercalation and high volumetric capacitance of two-dimensional titanium carbide, Science 341 (6153) (2013) 1502–1505.
[59] E.S. Muckley, M. Naguib, H.W. Wang, L. Vlcek, N.C. Osti, R.L. Sacci, X. Sang, R. R. Unocic, Y. Xie, M. Tyagi, E. Mamontov, K.L. Page, P.R.C. Kent, J. Nanda, I. N. Ivanov, Multimodality of Structural, Electrical, and Gravimetric Responses of Intercalated MXenes to Water, ACS Nano. 11 (2017) 11118–11126, https://doi.org/10.1021/ACSNANO.7B05264.
[60] Y.u. Xie, Y. Dall'Agnese, M. Naguib, Y. Gogotsi, M.W. Barsoum, H.L. Zhuang, P.R. C. Kent, Prediction and characterization of mxene nanosheet anodes for non-lithium-ion batteries, ACS Nano. 8 (9) (2014) 9606–9615.
[61] J. Hadler-Jacobsen, S.K. Schnell, The Importance of Stacking and Coordination for Li, Na, and Mg Diffusion and Intercalation in $Ti_3C_2T_2$ MXene, Adv. Mater. Interfaces. 9 (17) (2022) 2200014.
[62] P. Bärmann, M. Winter, J. Gonzalez-Julian, T. Placke, Solvent Co-Intercalation-Induced Activation and Capacity Fade Mechanism of Few-/Multi-Layered MXenes in Lithium Ion Batteries, Small. 17 (47) (2021) 2104130.
[63] K. Prenger, Y. Sun, K. Ganeshan, A. Al-Temimy, K. Liang, C. Dun, J.J. Urban, J. Xiao, T. Petit, A.C.T. van Duin, D. Jiang, M. Naguib, Metal Cation Pre-Intercalated $Ti_3C_2T_x$ MXene as Ultra-High Areal Capacitance Electrodes for Aqueous Supercapacitors, ACS Appl. Energy Mater. 5 (2022) 9373–9382, https://doi.org/10.1021/ACSAEM.2C00653.